

Design of a Robotic Fish Based on a Passive Flexible Mechanism*

Ben Lu, Yuzhuo Fu, Qianqian Zou, Sai Deng and Chao Zhou

*State Key Laboratory of Management and Control for Complex Systems, Institute of Automation, Chinese Academy of Sciences,
Beijing, China*
University of Chinese Academy of Sciences
Beijing, China

{luben2019, fuyuzhuo2019, zouqianqian2019, dengsai2012, chao.zhou}@ia.ac.cn

Abstract - In recent years, along with the rapid development of manufacturing, control, sensing and other technologies, biomimetic robotic fish has played an increasingly important role in marine exploration, underwater rescue, water quality monitoring and other fields. This paper designed a robotic fish based on a passive flexible mechanism to realize the fish-like propulsion function. The motion simulation of the designed transmission mechanism was carried out to get the actual curve of the structure. Through the analysis of the force of the fishtail, the preliminary selection scheme of the elastic joints based on the passive flexible mechanism was obtained. Finally, this paper built a robotic fish based on a passive flexible mechanism, which could achieve the motion frequency adjustable from 0.5 to 9 Hz, and the maximum swimming speed reaching 1.05 BL/s (BL, body length). This design scheme provided a new reference for the design of the biomimetic robotic fish and had certain practical significance.

Index Terms - Passive flexible mechanism, crank rocker mechanism, robotic fish.

I. INTRODUCTION

The ocean is rich in oil and gas resources, mineral resources and biological resources. Autonomous underwater vehicles (AUVs) play an increasingly important role in civil applications such as marine exploration, water quality monitoring, and military applications. In nature, fish have an extraordinary underwater movement talent. The special physiological structure and swimming mechanism of fish enable them to perform a variety of motion patterns such as rapid linear movement, rapid steering, and long-term parade with high efficiency. The comparison of statistical data [1] shows that the mobility of AUVs based on the traditional propeller is far less than that of these underwater creatures. If the artificial equipment can be used to reproduce and even surpass the excellent mobile performance of fish, it will have a profound impact on human development. Therefore, the research of underwater bionic robots has become more and more important.

From 2004 to 2010, Liu et al. from the University of Essex developed the MT series and G series of robotic fish [2]–[4]. The movement mode of the G9 series was BCF, with the rear fish body equipped with three servos to obtain propulsion. In terms of control methods, the G9 series used the

C-shaped starting equation (CST model) to achieve the steering of the fish body, and used the fish body wave equation to control the linear propulsion motion. The experimental results showed that the maximum turning velocity of the G9 series robotic fish was 130°/s, and the average turning velocity was 70°/s.

In 2008, Boston Engineering Corporation launched the SCOPE project based on the robotic fish GhostSwimmer [5], [6]. In addition, the BIOSwimmer as a variant of GS, equipped with a propeller at the tail, could achieve fast small-radius steering movement, and fast linear motion. Experimental data showed that the BIOS could reach a maximum forward speed of 5 knots and backward speed of 3 knots.

In 2014, Marchese et al. developed a soft robotic fish [7]. The experimental data showed that the robotic fish with a body length of 0.339 m achieved the maximum turning velocity of more than 300°/s and a linear velocity of 0.32 m/s in the S-start experiment.

In 2016, Bonnet et al. [8] developed a single-joint micro robotic fish to study the interaction between zebrafish and robotic fish. The fish body was about 8 cm long and achieved the maximum speed of 0.025 m/s.

From 2005 to 2011, Liang et al. successfully developed the third generation underwater vehicle SPC-III based on SPC and SPC-II series underwater robots, which resembled torpedo [9]. The SPC-III was 1.60 m long and used a 150 W DC servo motor for two-joint drive, which achieved the maximum speed of 1.36 m/s (0.85 BL/s).

From 2008 to 2010, Han et al. developed a four-joint robotic fish [10]. It was 0.6 m long and used carp as an imitation object. Han et al. studied the C-start behavior of fish based on the robotic fish. Experimental data showed that the robotic fish could achieve the maximum linear speed of 0.35 m/s (0.58 BL/s), a maximum steering angle of approximately 100°, and a maximum steering angular velocity of 110°/s.

From 2008 to 2010, Wang et al. developed a multimodal robotic fish [11]–[13]. The fish body was 0.6 m long and the control method was implemented by a CPG model based on Hopf oscillator. Experimental data showed that the robotic fish could achieve a forward speed of 0.27 m/s (0.45 BL/s) and backward speed of 0.18 m/s (0.3 BL/s).

* This work is partially supported by NSFC Grant 61903362 , Youth Innovation Promotion Association CAS (2019138) and the 2019 youth research fund of the State Key Laboratory of Management and Control for Complex Systems(20190201).

From 2010 to 2012, Su et al. developed a four-joint robotic fish and used this as a platform to study the rapid start-up behavior of fish [14], [15]. The experimental results showed that the designed four-joint robotic fish could achieve precise steering with a first steering error of less than 10°/s.

The robotic fish designed in this paper adopted a passive flexible mechanism in the propulsion structure. It used elastic mechanical components combined with the hydrodynamic force to realize the passive movement of the elastic joints and simulate the sinusoidal motion of the fish in nature. By using a single motor to drive the fishtail and a relatively simple motor control algorithm, the robotic fish could achieve high frequency propulsion and make full use of the performance of the motor. It achieved the motion frequency adjustable from 0.5 to 9 Hz, and the maximum swimming speed reaching 1.05 BL/s. This method provided a potential for the development of high-efficiency, low-noise, energy-saving and highly maneuverable underwater vehicles.

II. MECHANICAL DESIGN

The robotic fish designed in this paper used a single motor to drive the tail and the rotation of the motor was converted into the swing of the fishtail through the bevel gear set and the crank rocker mechanism. The fishtail adopted a passive flexible mechanism and was bent when subjected to the hydrodynamic force to simulate the sinusoidal motion of natural fish and realize the fish-like propulsion.

This method could achieve high frequency propulsion by using a single motor (see arrow 1 in Fig. 1) to drive the fishtail. As shown in Fig. 1, the rotation of the motor was converted into the swing of the fishtail by the mechanical structure. This design used a bevel gear set (see arrow 2 in Fig. 1) and a crank rocker mechanism (see arrow 3 in Fig. 1) to achieve motion conversion. The mechanical structure used in the experiment was shown in Fig. 1, where arrow 3 indicated a crank rocker mechanism with no snapback characteristics. Among them, through the bevel gear set and the crank rocker mechanism, the fishtail achieved a swing angle range of -20° to +20°.

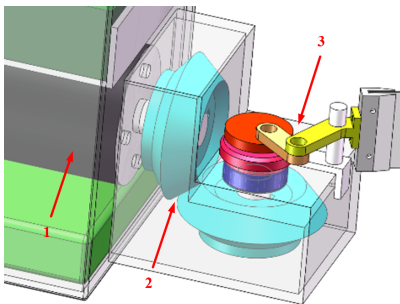


Fig. 1 Details of the transmission mechanism.

In this design, a few of passive flexible joints (elastic components) were used in series to form a fishtail structure, which relied on the hydrodynamic force to achieve passive bending and simulate the actual fish body wave curve. The fishtail structure was shown in Fig. 2, where the white parts were elastic joints and the black parts were hard plates.

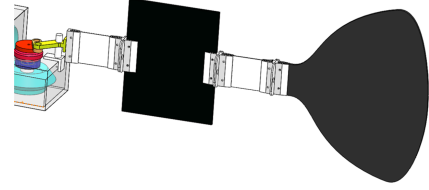


Fig. 2 Side view of the fishtail structure.

III. FORCE ANALYSIS AND SELECTION OF THE PASSIVE FLEXIBLE MECHANISM

The robotic fish was designed to realize the fish-like propulsion function. In this paper, it was expected that when the fishtail was subjected to the hydrodynamic force, each joint should be bent in a specific angle to realize the bionic swing of the fishtail. Therefore, it was necessary to choose suitable materials of the elastic joints. The elastic modulus of the materials was calculated and selected below.

To simplify the calculation, some simple initial conditions were assumed here. As shown in Fig. 3, it was assumed that the fishtail was swinging around the central symmetry position at this moment, when the angular velocity of each joint was the largest, each joint was subjected to the greatest hydrodynamic force, and the bending degree of the elastic joints were the largest. Therefore, this moment was taken as an example for analysis.

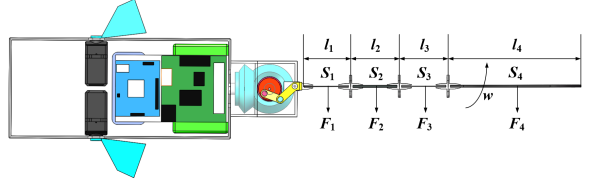


Fig. 3 Schematic diagram of force analysis of elastic components.

The thickness of each joint was 2 mm, and the hydrodynamic force perpendicular to the joints was F_i ($i = 1, \dots, 4$). It was assumed that the hydrodynamic force acted on the midpoint of each joint. At this moment, the fishtail swing frequency f was 1 Hz, and the length of each joint was: $l_1 = 30$ mm, $l_2 = 80$ mm, $l_3 = 30$ mm, $l_4 = 80$ mm. Since the force of each joint was mainly related to the area of the cross section, the length and width description of the sections in the vertical flow direction of the four joints were omitted here. The area corresponding to each joint was: $S_1 = 450 \text{ mm}^2$, $S_2 = 1200 \text{ mm}^2$, $S_3 = 450 \text{ mm}^2$, $S_4 = 6800 \text{ mm}^2$.

This paper used a common formula that was widely used to calculate the hydrodynamic force on vertical surfaces:

$$F = -\mu \operatorname{sgn}(v^\perp)(v^\perp)^2. \quad (1)$$

where, $\mu = \frac{1}{2} \rho C S$ was the drag coefficient, ρ was the fluid density, C was the shape factor, S was the effective area of each joint, and v^\perp was the normal projection of the swing velocity on the surface of the joint. Therein, fluid density here was water density, and the value of the shape factor was the empirical value of 1.1. For the l_1 segment in Fig. 3, the superposition method of the force and the torque at the end point (see Fig. 4) was used, and the calculation formulas of the cantilever beam deflection were combined:

$$\theta_B = -\frac{ml}{EI}. \quad (2)$$

$$\theta_B = -\frac{Pl^2}{2EI}. \quad (3)$$

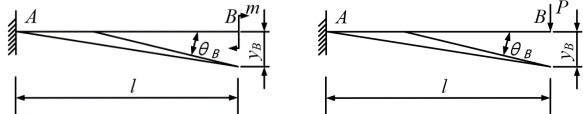


Fig. 4 Schematic diagram of the concentrated force of the cantilever beam.

Here, assuming $\theta_B = 30^\circ$, by combining the above formulas, the elastic modulus $E \approx 40.19$ GPa of the l_1 segment was obtained. The relationship between the fishtail swing frequency f and the required elastic modulus E of l_1 was shown in Fig. 5. It was shown that as the fishtail swing frequency f increased, the required elastic modulus E of l_1 gradually increased, which was in line with the actual situation.

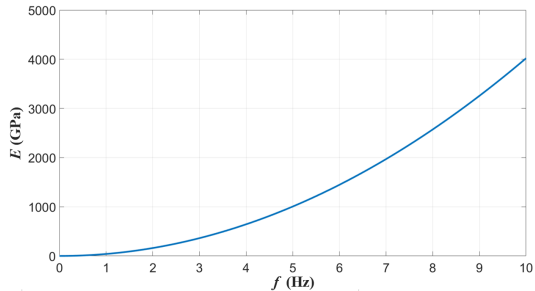


Fig. 5 Functional relationship between f and E .

After investigation, some common materials met the requirements of this paper such as nylon, nylon 1010, high-pressure polyethylene, etc. The selection of l_3 segment was the same. In this paper, nylon 1010 was used as the material of the elastic joints.

IV. THE MOTOR CONTROL ALGORITHM

The robotic fish was driven by a single motor, and the fishtail was expected to achieve the sinusoidal periodic swing. Among the many mechanisms that converted rotation into oscillation, the crank rocker was a relatively simple and commonly used mechanism. The enlarged view and equivalent schematic diagram of the crank rocker mechanism in this design was shown in Fig. 6.

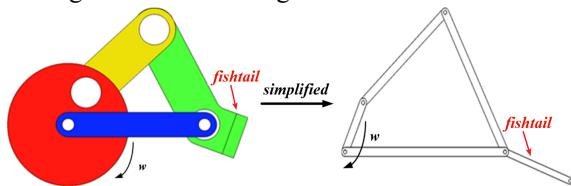


Fig. 6 The enlarged view and equivalent schematic diagram of the crank rocker mechanism.

The motion simulation of the crank rocker mechanism was shown in Fig. 7, where $l_1 = 6.0$ mm, $l_2 = 15.2121$ mm, $l_3 = 17.5428$ mm, $l_4 = 22.4312$ mm, $\theta_4 = 138^\circ$. The length of $l_1 \sim l_4$ was designed to meet the no quick-return characteristics. The minimum transmission angle was large, and the transmission efficiency was high.

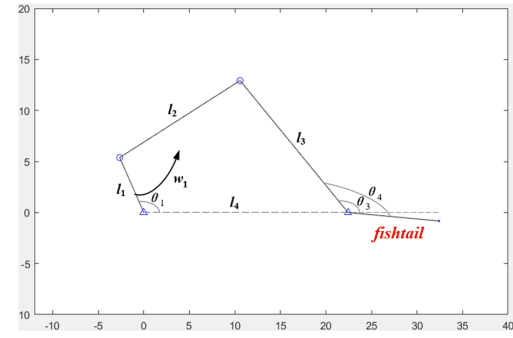


Fig. 7 Simulation diagram of the crank rocker mechanism.

In this paper, θ_1 was increased at a constant speed with the swing frequency $f = 1$ Hz. Part of the simulation process was shown in Fig. 8, and the curve of θ_3 was obtained as shown in Fig. 9.

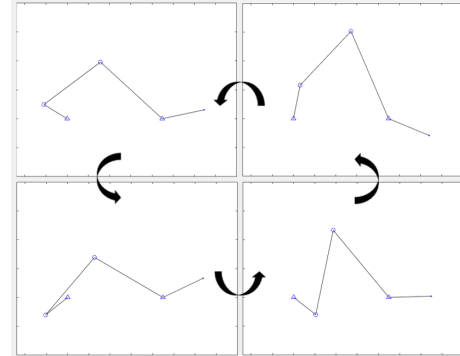


Fig. 8 Motion process of the crank rocker mechanism.

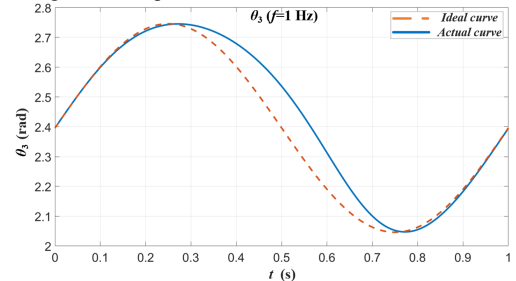


Fig. 9 Ideal and actual curve of θ_3 .

According to previous research experience, to achieve stable movement of the robotic fish, referring to Fig. 10, a reasonable control strategy was: when the fishtail swung around position 1, 3 (two endpoints), the angular velocity was 0 rad/s, and when it swung around position 2 (center position), the angular velocity was maximum, and the change of the angular velocity was sinusoidal, which meant the change of θ_3 (see Fig. 7) should follow the same rule. The specific solution was as follows.

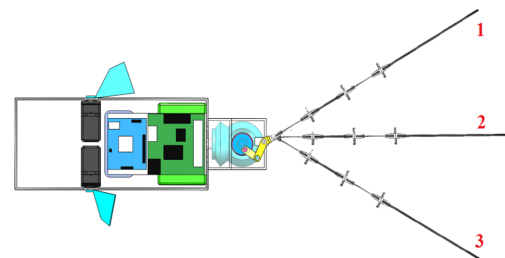


Fig. 10 Schematic diagram of the swing position of the fishtail.

Firstly, based on the above simulation result, the curve of θ_3 was obtained when θ_1 increased at a constant rate (the fishtail swung at a constant speed and the motor rotated at a constant speed), as shown in Fig. 9, where the dotted line was the ideal curve showing the standard sinusoidal variation, and the solid line was the actual curve, showing a similar sinusoidal variation.

After that, since the coordinates of each point of the curves were known, this paper directly used the coordinates as a database, and used the ideal sinusoidal variation of θ_3 to solve the ideal θ_1 corresponding to each moment. The result was shown in Fig. 11.

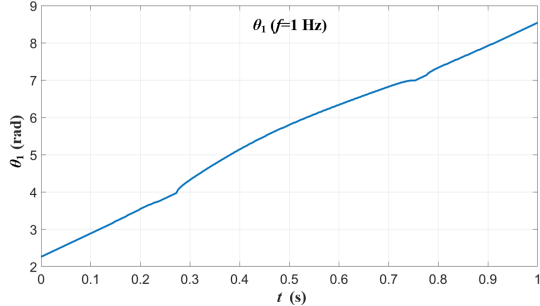


Fig. 11 Ideal curve of θ_1 .

Then, the above-mentioned variation of θ_1 was introduced into the crank rocker mechanism simulation model, and the actual variation of θ_3 was obtained, as shown in Fig. 12. It was shown that the actual variation curve of θ_3 was very close to the ideal curve, and the maximum error didn't exceed 1° , which verified the correctness of the solution.

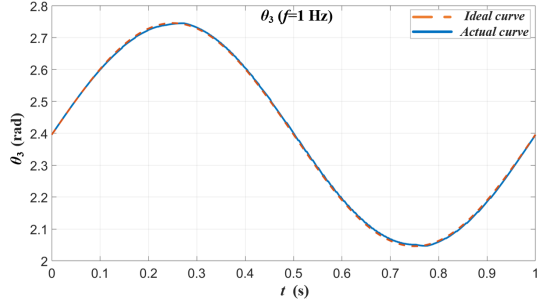


Fig. 12 Ideal and actual curve of θ_3 .

However, since the ideal θ_1 was a numerical solution, some mutations occurred at some moments, which was not conducive to motor control. Therefore, curve fitting using Fourier analysis was performed on θ_1 , and the result was shown in Fig. 13.

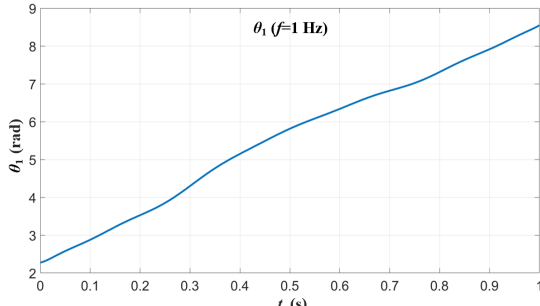


Fig. 13 Fitted curve of θ_1 .

The function of the fitted curve was:

$$\begin{aligned} \theta_1(t) = & 18.7 + 7.6 \cos(\omega t) - 23.8 \sin(\omega t) - 14.7 \cos(2\omega t) \\ & - 15.2 \sin(2\omega t) - 14.8 \cos(3\omega t) + 4.9 \sin(3\omega t) \\ & - 1.2 \cos(4\omega t) + 10.2 \sin(4\omega t) + 4.8 \cos(5\omega t) \\ & + 3.1 \sin(5\omega t) + 2.2 \cos(6\omega t) - 1.4 \sin(6\omega t) \\ & - 0.1 \cos(7\omega t) - 0.9 \sin(7\omega t) - 0.2 \cos(8\omega t) - 0.1 \sin(8\omega t) \end{aligned} . \quad (4)$$

where ω was the angular velocity, equal to 0.0063 rad/s . Then, this θ_1 was introduced into the simulation model, and the actual variation of θ_3 was obtained, as shown in Fig. 14. It was shown that the actual variation curve of θ_3 was very close to the ideal curve, and the maximum error didn't exceed 1° , which verified the correctness of the solution, and some mutations were removed, which was better than the direct numerical method in Fig. 11.

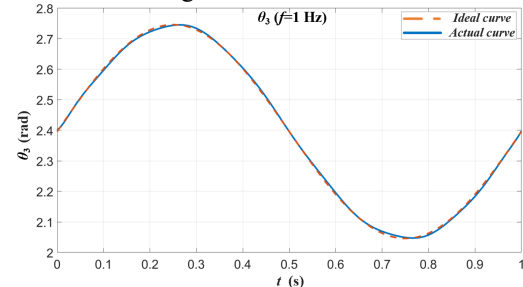


Fig. 14 Ideal and actual curve of θ_3 .

However, since (4) was very complicated, if the real-time calculation of θ_1 was used, the processing time of the program would be increased. In addition, if the curve was discretized, when the period of fishtail swing was small, the delay between the discrete points would gradually be similar to the delay caused by the program of controlling the motor speed itself, which would not be conducive to the realization of the sinusoidal swinging of the fishtail. Therefore, this design adopted the idea of compromise. For θ_1 , only the two most significant points and three zero points in one cycle on the sinusoid were fixed, and the other values were directly calculated by a piecewise linear function. The result of θ_1 was shown in Fig. 15.

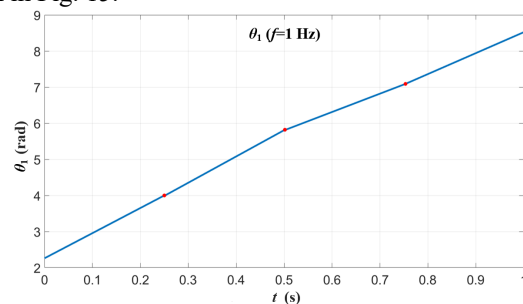


Fig. 15 Fitted curve of θ_1 by using a compromise method.

The function of the fitted curve by using a compromise method was:

$$\theta_1(t) = \begin{cases} 6.96t + 2.26 & t \in [0.00 \text{ s}, 0.25 \text{ s}] \\ 7.28t + 4.00 & t \in [0.25 \text{ s}, 0.50 \text{ s}] \\ 5.08t + 5.82 & t \in [0.50 \text{ s}, 0.75 \text{ s}] \\ 5.76t + 7.09 & t \in [0.75 \text{ s}, 1.00 \text{ s}] \end{cases} . \quad (5)$$

Then, this variation of θ_1 was introduced into the simulation model, and the actual variation of θ_3 was obtained, as shown in Fig. 16.

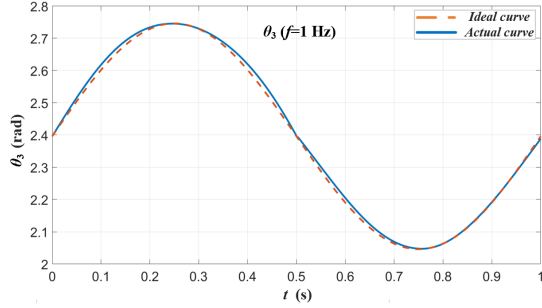


Fig. 16 Ideal and actual curve of θ_3 .

It was shown that the actual curve of θ_3 was also very close to the ideal curve, and the maximum error didn't exceed 1° , which verified the correctness of the solution. The calculation of this method was very simple, and all mutations were removed, which were very conducive to motor control.

V. EXPERIMENTAL RESULTS AND ANALYSIS

The robotic fish weighed 1.5 kg and was 37 cm long. The size of the test pool was 5×5 m, and a 1.3 megapixel color camera was installed above the center of the pool, which was used to collect information of the robotic fish.

In this experiment, the selected swing frequency f was between 0.5-9.0 Hz, and the step size was 0.5 or 1.0 Hz according to the actual situation. Each time the frequency was changed, the video of the robotic fish swimming process was recorded, and then an image processing program was used to analyze the video to obtain the average swimming speed and the trajectory of the robotic fish. Two experiments were conducted in this paper.

A. Two elastic joints experiment

The fishtail used in this experiment was the one shown in Fig. 2. This paper designed underwater experiments with multiple fishtail swing frequencies, and a video was recorded for each experiment. The video processing results were shown in Fig. 17.

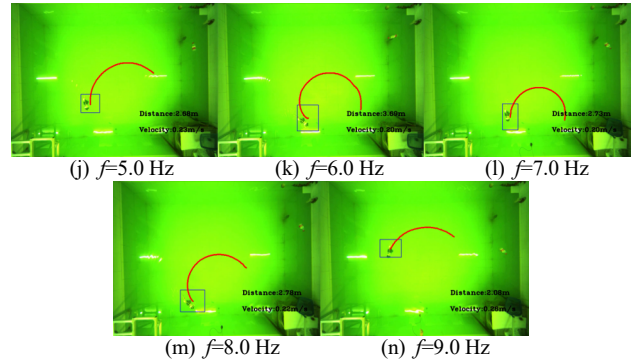
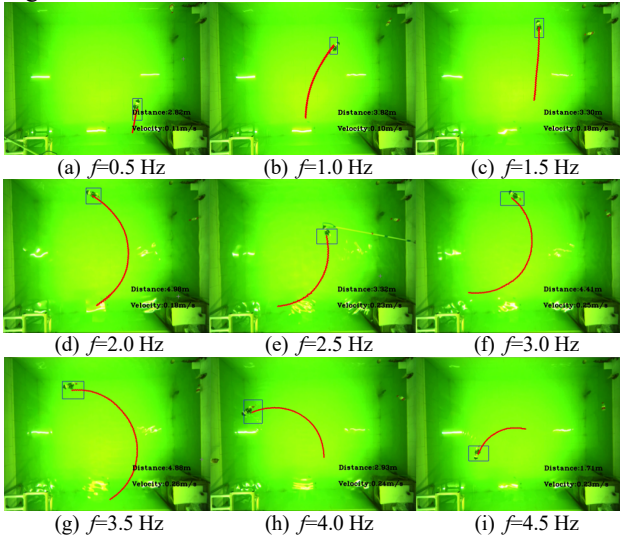


Fig. 17 Screenshot of the motion track at each swimming frequency.

The data of the swimming speed were extracted to obtain a frequency-swim speed curve, as shown in Fig. 18.

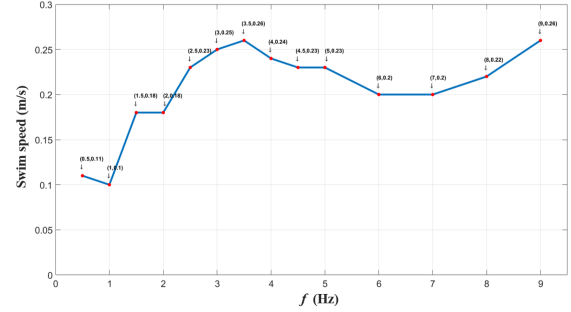


Fig. 18 Frequency-swim speed curve.

Analysis of the above data could lead to the following conclusions:

1) When the robotic fish with the fishtail of two elastic joints reached a certain swimming frequency, with the increase of the swimming frequency, the swinging amplitude of the fishtail and the propulsion efficiency gradually decreased, so the swimming speed gradually decreased. When the swimming frequency increased to a certain high value (6 Hz in this experiment), the increase of the propulsion efficiency caused by the increase of the swimming frequency was dominant, and the swimming speed gradually increased.

2) When the swing frequency f was bigger than 2 Hz, the maneuverability of the robotic fish with the fishtail of two elastic joints was good, and the relative swimming speed was above 0.5 BL/s. When the swing frequency was about 3.5 Hz or 9 Hz, the swimming speed was 0.26 m/s (0.7 BL/s), which was the maximum value.

B. Single elastic joint experiment

In the above experiment, the maximum speed of the robotic fish was 0.26 m/s, and the relative swimming speed was about 0.7 BL/s. Observing the experimental phenomena, it was found that the fishtail swing pattern changed under the condition of high swing frequency (above 5 Hz). Within a certain swing frequency range, as the swing frequency f increased, the swing amplitude of the fishtail gradually decreased, and the propulsion efficiency would reduce. Analysis of the experimental phenomena revealed that the main reason was that the nylon 1010 had a small elastic modulus which could not withstand such high-frequency periodic oscillation. In addition, the metal baseplate of the robotic fish was heavy, which also had a negative effect on the speed.

Based on the above analysis, in this experiment, the material of the elastic joints was changed to the alloy steel. The second elastic joint (J_2 in Fig. 3) was removed, and the metal baseplate was replaced by a plastic baseplate.

In this experiment, the selected swing frequency f was between 1.0–7.5 Hz, and the results were shown in Fig. 19.

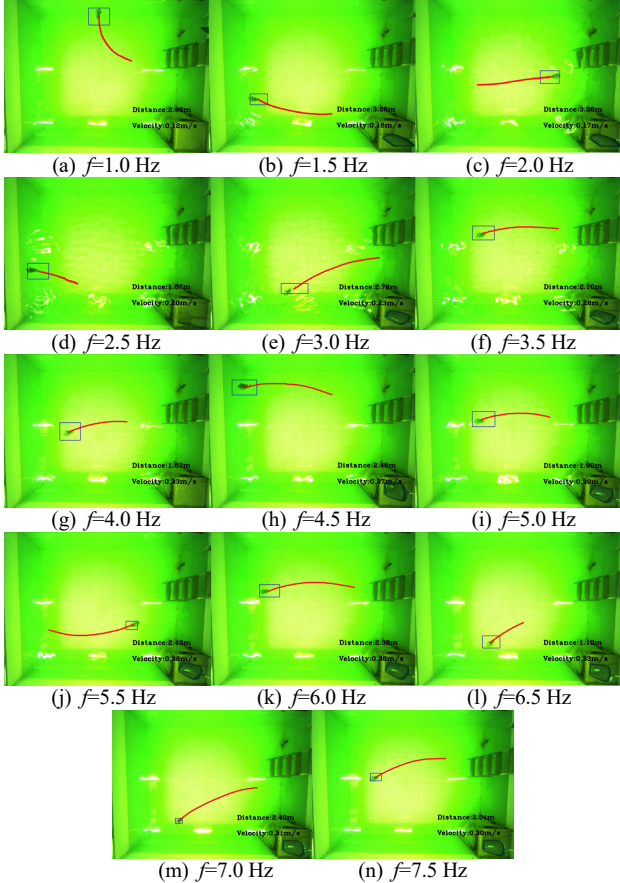


Fig. 19 Screenshot of the motion track at each swimming frequency.

The data of the swimming speed in the above results were extracted to obtain a frequency-swim speed curve, as shown in Fig. 20.

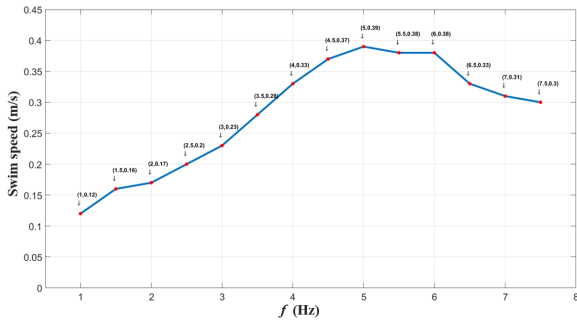


Fig. 20 Frequency-swim speed curve.

Analysis of the above data could lead to the following conclusions:

1) The elastic modulus of the elastic joints was an important factor affecting the maneuverability of the robotic fish. In addition, the number of the elastic joints and the weight of the robotic fish would affect the maneuverability of the robotic fish as well.

2) When the robotic fish with the fishtail of a single elastic joint reached a certain swimming frequency (5 Hz in this experiment), with the increase of the swimming frequency, the swinging amplitude of the fishtail and the propulsion efficiency gradually decreased, so the swimming speed gradually decreased.

3) When the swing frequency was above 2.5 Hz, the maneuverability of the robotic fish with the fishtail of a single elastic joint was good, and the speed/body length value was above 0.5 BL/s. When the swing frequency was about 5 Hz, the swimming speed was 0.39 m/s (1.05 BL/s), which was the maximum value.

VI. CONCLUSION AND FUTURE WORK

This paper proposed a fishtail structure of the robotic fish based on a passive flexible mechanism. The robotic fish was driven by a single motor, and the rotation of the motor was converted into a fishtail swing through the crank rocker mechanism, which could achieve a high swing frequency. The method of motor control was relatively simple, so the performance of the motor could be well utilized, which meant the propulsion efficiency could be improved. It was shown from the experiments that the maximum relative swimming speed of the robotic fish reached 1.05 BL/s, which had certain practical significance and great potential for improvement. It laid the foundation for the research and development of the efficient and highly maneuverable robotic fish based on passive flexible mechanisms.

In the future, we plan to perform more in-depth mechanical and kinematic modeling of the passive flexible mechanism. We also intend to optimize the mechanical structure of robotic fish and do more experiments to study the main factors affecting the performance of robotic fish.

REFERENCES

- [1] A. J. Murphy and M. Haroutunian, "Using bio-inspiration to improve capabilities of underwater vehicles," in *17th International Unmanned Untethered Submersible Technology Conference*, pp. 20–31, 2011.
- [2] J. Liu and H. Hu, "Mimicry of sharp turning behaviours in a robotic fish," in *Proceedings of the 2005 IEEE International Conference on Robotics and Automation (ICRA)*, Barcelona, Spain, pp. 3318–3323, Apr. 2005.
- [3] H. Hu, J. Liu, I. Dukes, and G. Francis, "Design of 3-D swim patterns for autonomous robotic fish," in *Proceedings of 2006 IEEE/RSJ International Conference on Intelligent Robots and Systems*, Beijing, China, pp. 2406–2411, Oct. 2006.
- [4] J. Liu and H. Hu, "Biological inspiration: from carangiform fish to multi-joint robotic fish," *Journal of Bionic Engineering*, 7(1):35–48, 2010.
- [5] M. Conry, A. Keefe, W. Ober, M. Rufo, and D. Shane, "Bioswimmer: Enabling technology for port security," in *Proceedings of 2013 IEEE International Conference on Technologies for Homeland Security (HST)*, Waltham, MA, pp. 364–368, 2013.
- [6] M. M. Rufo, "GhostswimmerTM: Tactically relevant, biomimetically inspired, silent, highly efficient and maneuverable autonomous underwater vehicle," Distribution Statement A—Approved for Public Release, Boston Engineering Corporation. <http://auvac.org>.
- [7] A. D. Marchese, C. D. Onal, and D. Rus, "Autonomous soft robotic fish capable of escape maneuvers using fluidic elastomer actuators," *Soft Robotics*, 1(1):75–87, 2014.
- [8] F. Bonnet, Y. Kato, J. Halloy, and F. Mondada, "Infiltrating the zebrafish swarm: design, implementation and experimental tests of a

- miniature robotic fish lure for fish–robot interaction studies,” *Artificial Life and Robotics*, 21(3): 239–246, 2016.
- [9] J. Liang, T. Wang, and L. Wen, “Development of a two-joint robotic fish for realworld exploration,” *Journal of Field Robotics*, 28(1):70–79, 2011.
 - [10] Q. Yan, Z. Han, S. Zhang, and J. Yang, “Parametric research of experiments on a carangiform robotic fish,” *Journal of Bionic Engineering*, 5(2):95–101, 2008.
 - [11] M. Wang, J. Yu, M. Tan, and J. Zhang, “Multimodal swimming control of a robotic fish with pectoral fins using a CPG network,” *Chinese Science Bulletin*, 57(10):1209– 1216, 2012.
 - [12] M. Wang, J. Yu and M. Tan, “Modeling neural control of robotic fish with pectoral fins using a CPG-based network,” in *Proceedings of the 48h IEEE Conference on Decision and Control (CDC) held jointly with 2009 28th Chinese Control Conference*, Shanghai, 2009, pp. 6502-6507.
 - [13] J. Yu, M. Wang, W. Wang, M. Tan and J. Zhang, “Design and control of a fish-inspired multimodal swimming robot,” *2011 IEEE International Conference on Robotics and Automation*, Shanghai, 2011, pp. 3664-3669.
 - [14] Z. Su, J. Yu, M. Tan, and J. Zhang, “Implementing flexible and fast turning maneuvers of a multijoint robotic fish,” *IEEE/ASME Transactions on Mechatronics*, 99:1–10, 2013.
 - [15] Z. Su, J. Yu, M. Tan and J. Zhang, “A closed-loop method to generate fast C-start for a robotic fish,” *2011 IEEE International Conference on Mechatronics and Automation*, Beijing, 2011, pp. 365-370.